

# Tight binding analysis of Si and GaAs ultra thin bodies with subatomic resolution

Yaohua P. Tan,<sup>1,\*</sup> Michael Povolotskyi,<sup>1</sup> Tillmann Kubis,<sup>1</sup> Timothy B. Boykin,<sup>2</sup> and Gerhard Klimeck<sup>1</sup>

<sup>1</sup>*School of Electrical and Computer Engineering, Network for Computational Nanotechnology,  
Purdue University, West Lafayette, Indiana, USA, 47906*

<sup>2</sup>*Department of Electrical and Computer Engineering,  
University of Alabama in Huntsville, Huntsville, Alabama 35899 USA*

(Dated: March 17, 2015)

Empirical tight binding (ETB) methods are widely used in atomistic device simulations. Traditional ways of generating the ETB parameters rely on direct fitting to bulk experiments or theoretical electronic bands. However, ETB calculations based on existing parameters lead to unphysical results in ultra small structures like the As terminated GaAs ultra thin bodies (UTBs). In this work, it is shown that more reliable parameterizations can be obtained by a process of mapping *ab-initio* bands and wave functions to tight binding models. This process enables the calibration of not only the ETB energy bands but also the ETB wave functions with corresponding *ab-initio* calculations. Based on the mapping process, ETB model of Si and GaAs are parameterized with respect to hybrid functional calculations. Highly localized ETB basis functions are obtained. Both the ETB energy bands and wave functions with subatomic resolution of UTBs show good agreement with the corresponding hybrid functional calculations. The ETB methods can then be used to explain realistically extended devices in non-equilibrium that can not be tackled with *ab-initio* methods.

PACS numbers:

## I. INTRODUCTION

Modern semiconductor nanodevices have reached critical device dimensions in the sub-10 nanometer range. These devices consist of complicated two or three dimensional geometries and are composed of multiple materials. Confined geometries such as ultra thin body (UTB),<sup>1</sup> FinFETs<sup>2</sup> and nanowires<sup>3</sup> structures are usually adopted in nanometer scale device designs to obtain desired performance characteristics. Most of the electrically conducting devices are not arranged in infinite periodic arrays, but are of finite extent with contacts controlling the current injections and potential modulation. Typically, there are about 10000 to 10 million atoms in the active device region with contacts controlling the current injection. These finite sized structures suggest an atomistic, local and orbital-based electronic structure representation for device level simulation. Quantitative device design requires the reliable prediction of the materials' band gaps and band offsets within a few meV and important effective masses within a few percent in the geometrically confined active device regions. ETB model is usually fitted to bulk dispersions without any definition of the spatial wave function details. However, recent *ab-initio* study of UTBs<sup>4</sup> showed that the surface carrier distribution in confined systems is strongly geometry and material dependent. This suggests that the charge distribution for realistic predictions of nanodevice performances should be resolved with subatomic resolution.

*Ab-initio* methods offer atomistic representations with subatomic resolution for a variety of materials. However, accurate *ab-initio* methods, such as Hybrid functionals,<sup>5</sup> GW<sup>6</sup> and BSE approximations<sup>7</sup> are in general computationally too expensive to be applied to systems containing millions of atoms. Furthermore, those methods assume equilibrium and cannot truly model out-of-equilibrium

device conditions where e.g. a large voltage might have been applied to drive carriers. The ETB methods are numerically much more efficient than *Ab-initio* methods. ETB has established itself as the standard state-of-the-art basis for realistic device simulations. It has been successfully applied to electronic structures of millions of atoms<sup>8</sup> as well as on non-equilibrium transport problems that even involve inelastic scattering.<sup>9</sup> The accuracy of the ETB methods depend critically on the careful calibration of the empirical parameters. The traditional way to determine the ETB parameters is to fit ETB band structures to experimental data of bulk materials.<sup>10,11</sup>

The ETB basis functions remain implicitly defined during traditional fitting processes. The lack of explicit basis functions makes it difficult to predict wave function dependent quantities like optical matrix elements with high precision. More importantly, ETB models parameterized by traditional fitting processes suffer from potential ambiguity when applied to ultra small structures such as UTBs, nanowires and more complicated geometries. For instance, the existing ETB parameters of GaAs<sup>11</sup> applied to a As terminated GaAs UTB with an implicit Hydrogen passivation model<sup>12</sup> results in unphysical top valence band states as shown in Fig. 1: The real space probability amplitudes of *ab-initio* topmost valence bands correspond to confined states with the probability amplitude peaking in the center of the UTB rather than the surface of the UTB as in ETB. In Fig. 1, the hybrid functional calculations include Hydrogen atoms explicitly whereas the ETB calculations include only their impact implicitly.<sup>12</sup> The mismatch between the envelopes of ETB and *ab-initio* wavefunctions suggests a calibration of wave functions in the ETB parameterization process is necessary. It is also found that the method of passivation (i.e. implicit or explicit inclusion of Hydrogen atoms) has an

effect on the nature of the valence band states.

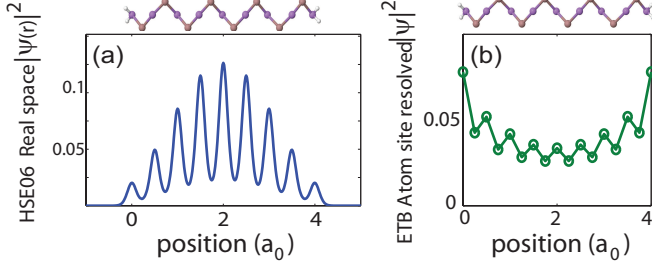


FIG. 1: In As terminated GaAs UTBs, hybrid functional probability amplitudes (a) of the top valence bands are confined states with probability amplitude peaking in the center of the UTB, while the ETB valence states (b) are surface states.

Therefore, a more fundamental fitting process that relates both the band structure and the wave functions of ETB models with *ab-initio* calculations is desirable. Existing approaches to construct localized basis functions and tightbinding-like Hamiltonians from *ab-initio* results include maximally localized Wannier functions (MLWF),<sup>13,14</sup> quasi-atomic orbitals,<sup>15,16</sup> or DFT-TB analysis.<sup>17</sup> The MLWFs are constructed using Bloch states of either isolated bands<sup>13</sup> or entangled bands.<sup>14</sup> These methods typically include interatomic interactions beyond first nearest neighbors. However, these methods do not eliminate the above discussed ambiguity of the commonly used orthogonal sp<sup>3</sup>d<sup>5</sup>s\* ETB models. Furthermore, these approaches usually disregard excited orbitals which are often needed to correctly parameterize semiconductors conduction bands. In previous work, it was already suggested how to generate ETB parameters that are compatible with typical ETB models and still reproduce *ab-initio* results.<sup>18</sup> This previous method was already applied to several materials such as GaAs, MgO<sup>18</sup> and SmSe<sup>19</sup> and yielded a good agreement between bulk ETB and *ab-initio* band structures. However, the resulting wave functions did not satisfactorily agree with the *ab-initio* wave functions.

In this paper, an improved algorithm of Ref.18 is presented that “maps” *ab-initio* results (i.e. eigenenergies and eigenfunctions) to tight binding models. Compared with the previous work,<sup>18</sup> the presented method allows much better agreement of the ETB and *ab-initio* wave functions. In this present mapping algorithm, rigorous, wavefunction-derived ETB parameters for the Hamiltonian, for highly localized basis functions, and for explicit surface passivation are obtained. It is important to mention that the ETB Hamiltonian of this method can be limited to first nearest neighbor interaction. The mapping process is applied to both bulk Si and GaAs to generate ETB parameters and explicit basis functions from corresponding hybrid functional calculations. It is demonstrated in this work, that the wave-function derived ETB Hamiltonian does not yield the ambiguity dis-

cussed with Fig. 1. In the same way, the transferability of the ETB model to nanostructures is improved. This is demonstrated by a comparison of ETB and Hybrid functional results in GaAs and Si UTBs.

This paper is organized as follows. In section II, the algorithm of parameter mapping from *ab-initio* calculations to tight binding models is described. Section III shows the application of the mapping algorithm to bulk and UTB systems. Subsection III A presents the application of the present algorithm to bulk Si and GaAs. Bulk band structures and realspace basis functions are shown and discussed there as well. Subsection III B shows the application of the algorithm to UTB systems and compares ETB band structures and wave functions with corresponding *ab-initio* results. The algorithm and its results are summarized in Section IV.

## II. METHOD

### A. Parameter Mapping Algorithm

The algorithm of the parameter mapping from *ab-initio* results to ETB models is shown in Fig. 2. As will be shown in the following, the ETB parameters and basis functions are obtained in an iterative fitting procedure that spans over 5 steps (with steps 3 through 4 being iterated). The resulting 1st nearest neighbor Hamiltonian  $\hat{H}^{TB}(\mathbf{k})$  is of Slater Koster table type.<sup>20,21</sup> The resulting basis  $\mathfrak{B}_{\text{final}}$  is composed of orthonormal real space functions  $\mathfrak{B}_{\text{final}} = \{\Psi_{n,l,m}^{\text{final}}(\mathbf{r})\}$  which have the shape (vectors are given in bold type)

$$\Psi_{a,n,l,m}(\mathbf{r}) = \bar{Y}_{l,m}(\theta, \phi) \bar{R}_{a,n,l}(r) + \sum_{\substack{l',m' \\ (l',m') \neq (l,m)}} \bar{Y}_{l',m'}(\theta, \phi) \tilde{R}_{a,n,l,l',m'}(r). \quad (1)$$

Here,  $a$  labels the atom type, whereas the  $n$ ,  $l$  and  $m$  are principle, angular and magnetic quantum numbers, respectively. All materials considered in this work contain no magnetic polarization. Therefore, the basis functions are spin independent. The tesseral spherical harmonics  $\bar{Y}_{l,m}(\theta, \phi)$  describe the dependence of the basis functions on the angular coordinates  $\theta$  and  $\phi$ . The functions  $\bar{R}_{a,n,l}(r)$  and  $\tilde{R}_{a,n,l,l',m'}(r)$  define the radial  $r$  dependence of the basis functions. The contribution of  $\tilde{R}_{a,n,l,l',m'}$  to the basis functions is much smaller than the contribution of  $\bar{R}_{a,n,l}$ . The detailed shapes of the radial functions  $\bar{R}_{a,n,l}(r)$  and  $\tilde{R}_{a,n,l,l',m'}(r)$  are subject to the fitting algorithm.

**Step 1:** First, electronic band structures  $\varepsilon_j^{Ab}(\mathbf{k})$  and wave functions  $\psi_{j,\mathbf{k}}^{Ab}$  are solved which serve as fitting targets to the overall mapping algorithm

$$\hat{H}^{Ab}(\mathbf{k}) |\psi_{j,\mathbf{k}}^{Ab}\rangle = \varepsilon_j^{Ab}(\mathbf{k}) |\psi_{j,\mathbf{k}}^{Ab}\rangle. \quad (2)$$

The index  $j$  corresponds to the band index and  $\mathbf{k}$  represents a momentum vector in the first Brillouin zone. In principle, any method that is capable of solving band

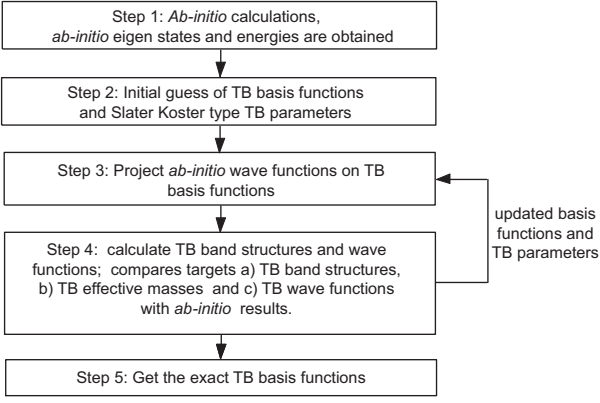


FIG. 2: The process of mapping from *ab-initio* calculations to Tight Binding by which the ETB parameters and ETB basis functions are extracted iteratively.

diagrams and explicit basis functions can provide these fitting targets. Throughout this work, however, hybrid functional calculations are performed for step 1.<sup>22</sup>

**Step 2:** In the second step, initial guesses for the ETB basis functions and ETB parameters are defined. During the fitting process, the ETB basis  $\mathfrak{B}_{\text{initial}}$  is spanned by non-orthogonal functions  $\{\Phi_{a,n,l,m}(\mathbf{r})\}$  given by

$$\Phi_{a,n,l,m}(\mathbf{r}) = \bar{Y}_{l,m}(\theta, \phi) R_{a,n,l}(r). \quad (3)$$

The  $R_{a,n,l}(r)$  in Eq. (3) differ from the  $\bar{R}_{a,n,l}(r)$  of the final basis functions in Eq. (1). The details of the initial guesses for the diagonal and off-diagonal elements of the Hamiltonian  $\hat{H}^{TB}(\mathbf{k})$  are not essential for the overall algorithm. Nevertheless, initial guesses that follow the framework of existing ETB parameter sets improve the overall fitting convergence. Urban et al. and Lu et al. discuss that interactions up to third nearest neighbors might be needed to exactly reproduce *ab-initio* results.<sup>16,17</sup> In contrast, we find that the interatomic interaction elements of  $\hat{H}^{TB}(\mathbf{k})$  can be limited to first nearest neighbor interactions throughout this work while still reproducing *ab-initio* results very well.

**Step 3:** The nonorthogonal basis functions  $\Phi_{a,n,l,m}(\mathbf{r})$  in position space are transformed into the Bloch representation<sup>23</sup>  $\Phi_{a,n,l,m,\mathbf{k}}(\mathbf{r})$

$$\begin{aligned} |\Phi_{\alpha,\mathbf{k}}\rangle &\equiv \Phi_{a,n,l,m,\mathbf{k}}(\mathbf{r}) \\ &= \sum_{\mathbf{R}} \exp[i\mathbf{k} \cdot (\mathbf{R} + \boldsymbol{\tau}_a)] \Phi_{a,n,l,m}(\mathbf{r} - \mathbf{R} - \boldsymbol{\tau}_a) \end{aligned} \quad (4)$$

where  $\boldsymbol{\tau}_a$  is the position of atom type  $a$  in the unit cell and the sum runs over all unit cells of the system with  $\mathbf{R}$ , the position of the respective cell. To improve readability of all formulas in the Dirac notation, the indices of atom type and quantum numbers are merged into Greek indices  $\alpha = (a, n, l, m)$ . For the further steps, an orthogonal basis  $\mathfrak{B}_{\text{ortho}} = \{|\Psi_{\alpha,\mathbf{k}}\rangle\}$  is created out of the basis  $\mathfrak{B}_{\text{initial}}$  with Löwdin's symmetrical orthogonalization algorithm.<sup>24</sup> Since steps 4 and 5 are formulated in the basis

$\mathfrak{B}_{\text{ortho}}$ , the wave functions  $|\psi_{j,\mathbf{k}}^{Ab}\rangle$  of step 1 must be transformed into this basis

$$|\psi_{j,\mathbf{k}}^{Ab}\rangle \approx \hat{P}(\mathbf{k}) |\psi_{j,\mathbf{k}}^{Ab}\rangle = \sum_{\alpha} c_{j,\alpha}(\mathbf{k}) |\Psi_{\alpha,\mathbf{k}}\rangle, \quad (5)$$

where

$$c_{j,\alpha}(\mathbf{k}) = \langle \Psi_{\alpha,\mathbf{k}} | \psi_{j,\mathbf{k}}^{Ab} \rangle, \quad (6)$$

$c_{j,\alpha}(\mathbf{k}) = \langle \Psi_{\alpha,\mathbf{k}} | \psi_{j,\mathbf{k}}^{Ab} \rangle$ , with the projection operator

$$\hat{P}(\mathbf{k}) = \sum_{\alpha} |\Psi_{\alpha,\mathbf{k}}\rangle \langle \Psi_{\alpha,\mathbf{k}}|. \quad (7)$$

Equation (5) contains an approximation of the *ab-initio* wave functions in so far that the sum over  $\alpha$  extends only over those orbitals that are included in the tight binding basis  $\mathfrak{B}_{\text{ortho}}$ . This basis and  $\mathfrak{B}_{\text{ortho}}$  of similar ETB models have much fewer basis vectors than the input *ab-initio* calculation. This rank reduction is a typical outcome of rectangular transformations such as  $\hat{P}$  and is well known in the field of low rank approximations.<sup>25</sup>

**Step 4:** Here, the quality of the ETB fitting is assessed. In this step, the band structures of the current ETB model  $\varepsilon_j^{TB}(\mathbf{k})$  and the *ab-initio* input  $\varepsilon_j^{Ab}(\mathbf{k})$  are compared. If these sufficiently agree, the phases of the ETB wave functions are modulated to agree with the *ab-initio* ones and both wave functions are compared after that. The ETB Hamiltonian of step 2 is diagonalized in the basis  $\mathfrak{B}_{\text{ortho}}$  of step 3 to obtain ETB band structures  $\varepsilon_j^{TB}(\mathbf{k})$  and eigen vectors  $|\psi_{j,\mathbf{k}}^{TB}\rangle$

$$\hat{H}^{TB}(\mathbf{k}) |\psi_{j,\mathbf{k}}^{TB}\rangle = \varepsilon_j^{TB}(\mathbf{k}) |\psi_{j,\mathbf{k}}^{TB}\rangle, \quad (8)$$

with

$$|\psi_{j,\mathbf{k}}^{TB}\rangle = \sum_{\alpha} d_{j,\alpha}(\mathbf{k}) |\Psi_{\alpha,\mathbf{k}}\rangle. \quad (9)$$

To assess the quality of the ETB results is assessed, different fitness functions  $F_{\varepsilon}$ ,  $F_m$  and  $F_{\psi}$  are defined for energies, masses and wave functions respectively. The  $F_{\varepsilon}$  and  $F_m$  are given by

$$F_{\varepsilon} = \sum_{j,\mathbf{k}} w_j^{\varepsilon}(\mathbf{k}) |\varepsilon_j^{TB}(\mathbf{k}) - \varepsilon_j^{Ab}(\mathbf{k})|^2. \quad (10)$$

$$F_m = \sum_m w_m \left| \frac{m^{Ab} - m^{TB}}{m^{Ab}} \right|^2. \quad (11)$$

where  $w_j^{\varepsilon}(\mathbf{k})$  and  $w_m$  are weights defined for each target.

As a convention for wave functions phases, another set of ETB wave functions  $|\tilde{\psi}_{j,\mathbf{k}}^{TB}\rangle$  is introduced

$$|\tilde{\psi}_{j,\mathbf{k}}^{TB}\rangle = \sum_i V_{j,i}(\mathbf{k}) |\psi_{i,\mathbf{k}}^{TB}\rangle. \quad (12)$$

The unitary transformation  $\hat{V}(\mathbf{k})$  is defined by

$$V_{j,i}(\mathbf{k}) = \frac{\langle \psi_{j,\mathbf{k}}^{TB} | \psi_{i,\mathbf{k}}^{Ab} \rangle}{\lambda(\mathbf{k})}, \quad (13)$$

with

$$\lambda(\mathbf{k}) = \sqrt{\frac{1}{N} \sum_{q,p} |\langle \psi_{q,\mathbf{k}}^{Ab} | \psi_{p,\mathbf{k}}^{TB} \rangle|^2}. \quad (14)$$

Here, the sum over  $p$  and  $q$  runs over all  $N$  ETB states  $|\psi_{p,\mathbf{k}}^{TB}\rangle$  and  $N$  *ab-initio* states  $\langle \psi_{q,\mathbf{k}}^{Ab} |$  with equivalent energies  $\varepsilon_p^{TB}(\mathbf{k}) \approx \varepsilon_q^{Ab}(\mathbf{k})$ . With this transformation, the equation holds

$$\langle \psi_{i,\mathbf{k}}^{Ab} | \psi_{j,\mathbf{k}}^{TB} \rangle = \lambda(\mathbf{k}), \quad (15)$$

for equivalent states. This phase adaption can only work if the ETB band structure is close enough to the *ab-initio* result. The ETB wave function fitness is given by

$$F_\psi = \sum_{j,\mathbf{k}} w_j^\psi(\mathbf{k}) \left\| |\psi_{j,\mathbf{k}}^{Ab}\rangle - |\tilde{\psi}_{j,\mathbf{k}}^{TB}\rangle \right\|^2. \quad (16)$$

The weights  $w_j^\psi(\mathbf{k})$  are varying depending on respective fitting focusses. Deviations of  $|\tilde{\psi}_{\nu,\mathbf{k}}^{TB}\rangle$  from  $|\psi_{\nu,\mathbf{k}}^{Ab}\rangle$  have in general two reasons: inadequate basis functions and/or eigenfunctions of a poorly approximated ETB Hamiltonian. Therefore,  $F_\psi$  can be estimated as

$$\begin{aligned} \left\| |\psi_{j,\mathbf{k}}^{Ab}\rangle - |\tilde{\psi}_{j,\mathbf{k}}^{TB}\rangle \right\|^2 &\leq 2 \left\| [\hat{I} - \hat{P}(\mathbf{k})] |\psi_{j,\mathbf{k}}^{Ab}\rangle \right\|^2 \\ &+ 2 \left\| \hat{P}(\mathbf{k}) |\psi_{j,\mathbf{k}}^{Ab}\rangle - |\tilde{\psi}_{j,\mathbf{k}}^{TB}\rangle \right\|^2. \end{aligned} \quad (17)$$

The first right hand side term of the last equation describes the deviation of the low-rank approximated *ab-initio* wave functions. This becomes obvious with the projector property  $\hat{P}^2(\mathbf{k}) = \hat{P}(\mathbf{k})$

$$\left\| [\hat{I} - \hat{P}(\mathbf{k})] |\psi_{j,\mathbf{k}}^{Ab}\rangle \right\|^2 = \langle \psi_{j,\mathbf{k}}^{Ab} | [\hat{I} - \hat{P}(\mathbf{k})] |\psi_{j,\mathbf{k}}^{Ab}\rangle. \quad (18)$$

The second term on the right hand side of Eq. (17) contains information about the quality of the eigenfunctions of the approximate ETB Hamiltonian  $\hat{H}^{TB}(\mathbf{k})$ . This is understandable when Eqs. (5) and (12) are inserted into this term

$$\begin{aligned} \left\| \hat{P}(\mathbf{k}) |\psi_{j,\mathbf{k}}^{Ab}\rangle - |\tilde{\psi}_{j,\mathbf{k}}^{TB}\rangle \right\|^2 &= \\ 2 - 2 \operatorname{Re} \left[ \sum_{\alpha,i} c_{j,\alpha}^\dagger(\mathbf{k}) V_{j,i}(\mathbf{k}) d_{i,\alpha}(\mathbf{k}) \right]. \end{aligned} \quad (19)$$

The fitness function  $F_\psi$  represents the major improvement over the traditional ETB eigenvalue fitting (e.g. typically limited to energies and effective masses). All fitness functions are minimized by iterating over the steps

3 and 4: the Slater Koster type parameters for the ETB Hamiltonian  $\hat{H}^{TB}(\mathbf{k})$  and the parameters of the radial ETB basis functions  $R_{a,n,l}(r)$  are adjusted for every iteration of step 3.

**Step 5:** Once the fitness functions are small enough to cease the iterations, it is assumed that those eigenfunctions of the ETB Hamiltonian  $\hat{H}^{TB}(\mathbf{k})$  that were subject to the fitting are identical to the eigenfunctions of the *ab-initio* Hamiltonian  $\hat{H}^{Ab}(\mathbf{k})$  after a transformation  $\hat{A}(\mathbf{k})$

$$|\psi_{j,\mathbf{k}}^{TB}\rangle \approx \sum_i A_{j,i}(\mathbf{k}) |\psi_{i,\mathbf{k}}^{Ab}\rangle. \quad (20)$$

This transformation  $\hat{A}$  is determined by a singular value decomposition of the rectangular overlap matrix of *ab-initio* eigenstates with ETB eigenstates

$$\langle \psi_{i,\mathbf{k}}^{Ab} | \psi_{j,\mathbf{k}}^{TB} \rangle = \sum_p U_{i,p}(\mathbf{k}) \Sigma_{p,p}(\mathbf{k}) W_{p,j}(\mathbf{k}). \quad (21)$$

The row index  $i$  runs over all *ab-initio* eigenstates - exceeding those that served as fitting targets, whereas the column index  $j$  covers all the ETB eigenfunctions. The  $\Sigma$  and  $W$  are square and  $U$  is a rectangular matrix. The transformation  $\hat{A}$  is then defined as

$$A_{j,i}(\mathbf{k}) = \sum_p W_{j,p}(\mathbf{k}) U_{p,i}^\dagger(\mathbf{k}). \quad (22)$$

$\hat{A}$  is constructed from relevant columns of a unitary transformation. Combining Eqs. (20) and (9) allows to determine the Bloch periodic final basis functions

$$|\Psi_{\alpha,\mathbf{k}}^{\text{final}}\rangle = \sum_{i,j} d_{\alpha,j}^\dagger(\mathbf{k}) A_{j,i}(\mathbf{k}) |\psi_{i,\mathbf{k}}^{Ab}\rangle. \quad (23)$$

The real space counterpart of  $|\Psi_{\alpha,\mathbf{k}}^{\text{final}}\rangle$  is given by

$$\Psi_\alpha^{\text{final}}(\mathbf{r} - \mathbf{R} - \boldsymbol{\tau}) = \frac{V}{(2\pi)^3} \int_{\text{BZ}} d\mathbf{k} e^{-i\mathbf{k} \cdot (\mathbf{R} + \boldsymbol{\tau})} \Psi_{\alpha,\mathbf{k}}^{\text{final}}(\mathbf{r}). \quad (24)$$

### III. RESULTS

In this work, *ab-initio* level calculations of Si and GaAs systems were performed with VASP.<sup>26</sup> The HSE06 hybrid functional<sup>22</sup> is used to produce reasonable band gaps in both the bulk and the UTB cases. In all HSE06 calculations, a cutoff energy of 350eV is used.  $\Gamma$ -point centered Monkhorst Pack kspace grids are used for both bulk and UTB systems. The size of the kspace grid for bulk calculations is a  $6 \times 6 \times 6$ , while one for UTB is  $6 \times 6 \times 1$ . k-points with integration weights equal to zero are added to the original  $6 \times 6 \times 6$  or  $6 \times 6 \times 1$  grids in order to generate energy bands with higher k-space resolution. The spin orbit coupling is included in band structure calculations. Small hydrostatic strains up to 0.3% are introduced to adjust the bulk band gaps in order to match experimental results. The lattice const used in this work is given by table I.

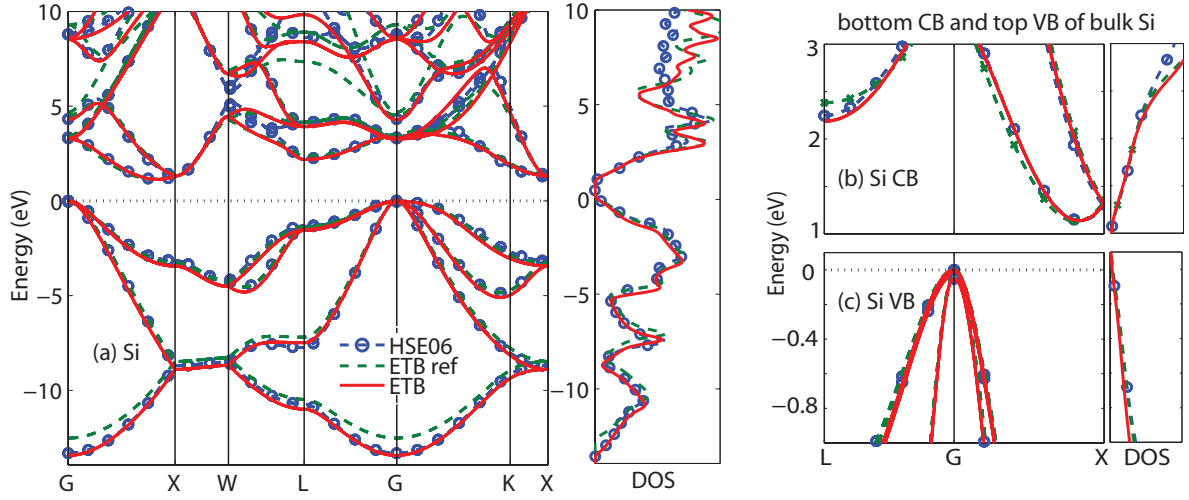


FIG. 3: Band structure and density of states of bulk Si. ETB band structure agree with the HSE06 band structure (a), especially for bottom conduction bands (b) and top valence bands(c) around Fermi level.

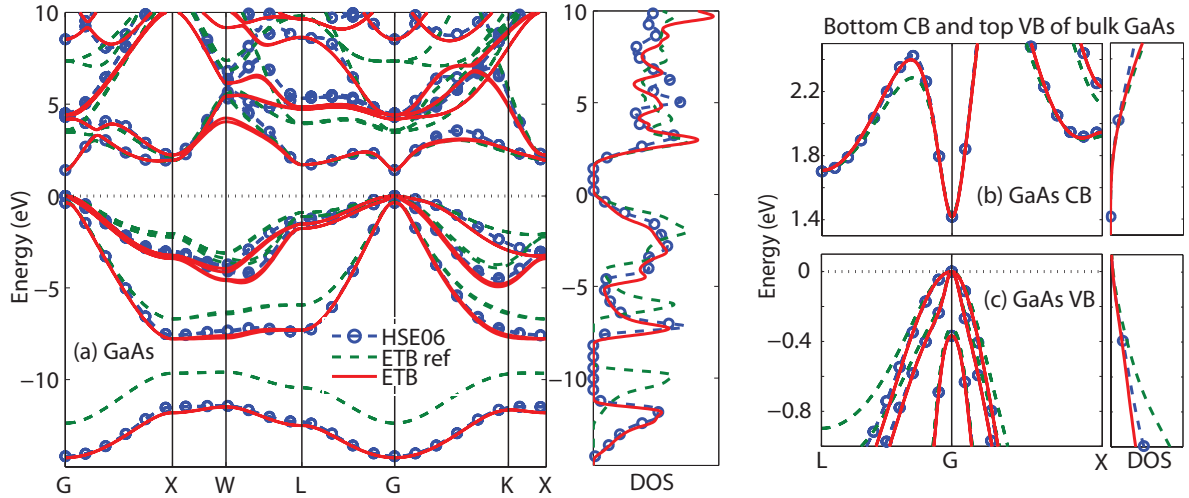


FIG. 4: Band structure and density of states of bulk GaAs. ETB band structure agree with the HSE06 band structure (a), especially for bottom conduction bands (b) and top valence bands(c) around Fermi level.

### A. Application to Bulk Materials

For bulk Si and GaAs, fitting targets include the band structures of the lowest 16 bands (with spin degeneracy) along high symmetry directions, important effective masses and wave functions at high symmetry points such as  $\Gamma$ ,  $L$  and  $X$  points. ETB basis functions in real space is reconstructed on  $6 \times 6 \times 6$   $\Gamma$  center  $k$  space grid using Eq (24).

The band structures and DOS of bulk Si and GaAs (HSE06 vs ETB) are shown in Fig. 3 and 4 respectively. The band structures using existing Si and GaAs ETB parameters<sup>11,27</sup> are also shown in corresponding figures. The ETB band structures and DOS using parameters generated by this work show better agreement with the

corresponding hybrid functional results compared with the existing parameterizations. For bulk Si, the existing parameterization shows a unexpected low  $s^*$  band around 5 eV above topmost valence bands. In the traditional fitting process, the  $s^*$  band shows a strong preference for moving downward.<sup>27</sup> Due to large number of parameters to be determined, traditional (energy-gap and effective-mass) based fitting procedures can find local minima in their fitness functions corresponding to wave functions significantly different from those predicted by *ab-initio* methods. The present method has the important advantage that optimization involves not only masses and gaps but also wavefunctions. Thus the ETB wavefunctions can be kept close to their *ab-initio* counterparts. For GaAs, the existing parameterization shows 2 eV higher  $s$ -type

Si		GaAs			
$a_0$	5.43Å	$a_0$	5.6307Å		
$E_s$	-2.803316	$E_{s_a}$	-8.063758	$E_{s_c}$	-1.603222
$E_p$	4.096984	$E_{p_a}$	3.126841	$E_{p_c}$	4.745896
$E_{s^*}$	25.163115	$E_{s_a^*}$	21.930865	$E_{s_c^*}$	23.630466
$E_d$	12.568228	$E_{d_a}$	13.140998	$E_{d_c}$	14.807586
$\Delta$	0.021926	$\Delta_a$	0.194174	$\Delta_c$	0.036594
$V_{ss\sigma}$	-2.066560	$V_{s_a s_c \sigma}$	-1.798514		
$V_{s^* s^* \sigma}$	-4.733506	$V_{s_a^* s_c^* \sigma}$	-4.112848		
$V_{ss^* \sigma}$	-1.703630	$V_{s_a s_c^* \sigma}$	-1.258382	$V_{s_c s_a^* \sigma}$	-1.688128
$V_{sp\sigma}$	3.144266	$V_{s_a p_c \sigma}$	3.116745	$V_{s_c p_a \sigma}$	2.776805
$V_{s^* p \sigma}$	2.928749	$V_{s_a^* p_c \sigma}$	1.635158	$V_{s_c^* p_a \sigma}$	3.381868
$V_{sd\sigma}$	-2.131451	$V_{s_a d_c \sigma}$	-0.396407	$V_{s_c d_a \sigma}$	-2.151852
$V_{s^* d \sigma}$	-0.176671	$V_{s_a^* d_c \sigma}$	-0.145161	$V_{s_c^* d_a \sigma}$	-0.810997
$V_{pp\sigma}$	4.122363	$V_{p_a p_c \sigma}$	4.034685		
$V_{pp\pi}$	-1.522175	$V_{p_a p_c \pi}$	-1.275446		
$V_{pd\sigma}$	-1.127068	$V_{p_a d_c \sigma}$	-1.478036	$V_{p_c d_a \sigma}$	-0.064809
$V_{pd\pi}$	2.383978	$V_{p_a d_c \pi}$	1.830852	$V_{p_c d_a \pi}$	2.829426
$V_{dd\sigma}$	-1.408578	$V_{d_a d_c \sigma}$	-1.216390		
$V_{dd\pi}$	2.284472	$V_{d_a d_c \pi}$	2.042009		
$V_{dd\delta}$	-1.541821	$V_{d_a d_c \delta}$	-1.829113		
$H_{Si}$		$H_c$ and $H_a$			
$E_{s_H}$	-3.056510	$E_{s_{H_c}}$	2.758428	$E_{s_{H_a}}$	-0.308397
$V_{s_H s_{Si} \sigma}$	-4.859509	$V_{s_{H_c} s_a \sigma}$	-2.960420	$V_{s_{H_a} s_c \sigma}$	-3.151427
$V_{s_H p_{Si} \sigma}$	3.776178	$V_{s_{H_c} p_a \sigma}$	5.490764	$V_{s_{H_a} p_c \sigma}$	3.539284
$V_{s_H s_{Si}^* \sigma}$	0.0	$V_{s_{H_c} s_a^* \sigma}$	0.0	$V_{s_{H_a} s_c^* \sigma}$	-0.129904
$V_{s_H d_{Si} \sigma}$	-0.007703	$V_{s_{H_c} d_a \sigma}$	-1.727690	$V_{s_{H_a} d_c \sigma}$	-0.252733
$\delta_{Si}$	-0.276789	$\delta_a$	-0.266815	$\delta_c$	-0.586952

TABLE I: Slater Koster type ETB parameters of bulk Si and GaAs, and passivation parameters of UTBs.

low lying valence bands. The ETB parameters of bulk Si and GaAs are listed in table I. It can be seen from tables II and III, the anisotropic hole masses by ETB show a remarkable agreement with HSE06 results. The principal authors of the previous works<sup>11,27</sup> explicitly pointed out that fitting hole masses had been very difficult with the previous methods.

The orthogonal ETB basis functions  $\mathfrak{B}_{\text{final}}$  of Si, Ga and As atoms are shown in Fig. 5. The ETB basis functions are slightly environment dependent because they are orthogonal. Thus the ETB basis functions are not invariant under arbitrary rotations but invariant under symmetry operations within  $T_d$  group, as pointed out by Slater and Koster.<sup>20</sup> It can be seen from Fig. 5.(a) to (f) that the  $s$  and  $p$  orbitals show  $s$  and  $p$  features near the atom. More complicated patterns in the area further away from the atom can be observed. These complicated patterns correspond to components with high angular momentums. The feature of orthogonal ETB basis function resembles the augmented basis functions used in *ab-initio* level calculations such as Augmented Plane Waves(APWs) and Muffin Tin Orbitals(MTOs). The orthogonal ETB basis functions have multiple angular parts in each orbital as shown by Fig. 5.(g),(h) and (i). The  $s$ ,  $p$  and  $d$  type ETB basis functions are dominated by components with  $l = 0, 1$  and  $2$  respectively. More than 90% for the  $s, p$  and  $d$  orbitals are comprised of

targets	Si			
	TB Ref	HSE06	TB	error (%)
$E_g(\Gamma)$	3.399	3.302	3.244	1.8
$E_g(X)$	1.131	1.142	1.139	0.2
$E_g(L)$	2.383	2.247	2.188	2.6
$\Delta_{SO}$	0.047	0.051	0.052	0.8
$m_{hh100}$	0.299	0.281	0.282	0.097
$m_{hh110}$	0.633	0.566	0.572	0.977
$m_{hh111}$	0.796	0.704	0.714	1.433
$m_{lh100}$	0.232	0.206	0.204	1.001
$m_{lh110}$	0.165	0.151	0.149	0.937
$m_{lh111}$	0.156	0.143	0.142	0.927
$m_{so100}$	0.266	0.244	0.242	0.809
$m_{so110}$	0.266	0.244	0.242	0.795
$m_{so111}$	0.267	0.244	0.242	0.770
$m_{cXl}$	0.887	0.928	0.857	7.615
$m_{cXt}$	0.225	0.207	0.215	3.544

TABLE II: Targets comparison of bulk Si. Critical band edges and effective masses at  $\Gamma$ ,  $X$  and  $L$  points by ETB and HSE06 calculations are compared.

targets	GaAs			
	TB Ref	HSE06	TB	error(%)
$E_g(\Gamma)$	1.424	1.418	1.416	0.2
$E_g(X)$	1.900	1.919	1.910	0.5
$E_g(L)$	1.707	1.702	1.708	0.3
$\Delta_{SO}$	0.326	0.368	0.367	0.1
$m_{hh100}$	0.383	0.310	0.337	8.510
$m_{hh110}$	0.667	0.573	0.619	7.879
$m_{hh111}$	0.853	0.750	0.813	8.507
$m_{lh100}$	0.085	0.082	0.083	0.744
$m_{lh110}$	0.078	0.073	0.074	1.614
$m_{lh111}$	0.076	0.071	0.072	1.715
$m_{so100}$	0.166	0.164	0.160	1.998
$m_{so110}$	0.166	0.164	0.160	2.037
$m_{so111}$	0.166	0.164	0.160	2.041
$m_{c100}$	0.068	0.065	0.067	2.787
$m_{c110}$	0.068	0.066	0.067	2.790
$m_{c111}$	0.068	0.065	0.067	2.781
$m_{cXl}$	1.526	1.577	1.480	6.142
$m_{cXt}$	0.177	0.215	0.204	5.083
$m_{cLl}$	1.743	1.626	1.446	11.055
$m_{cLt}$	0.099	0.111	0.136	22.614

TABLE III: Targets comparison of bulk GaAs. Critical band edges and effective masses at  $\Gamma$ ,  $X$  and  $L$  from TB and HSE06 calculations are compared.

their  $l = 0, 1$  and  $2$  components respectively. The excited  $s^*$  type ETB basis functions have higher angular momentum and the  $l = 0$  components have contributions of 60% to 70%. The second largest contribution in  $s^*$  orbitals is the  $f$  component with  $l = 3$ . The  $f$  component attached to the  $s^*$  orbitals have angular part equivalent to real space function  $xyz$ . This is a result of the existence of  $xyz$ -like crystal field near each atom in zincblende and



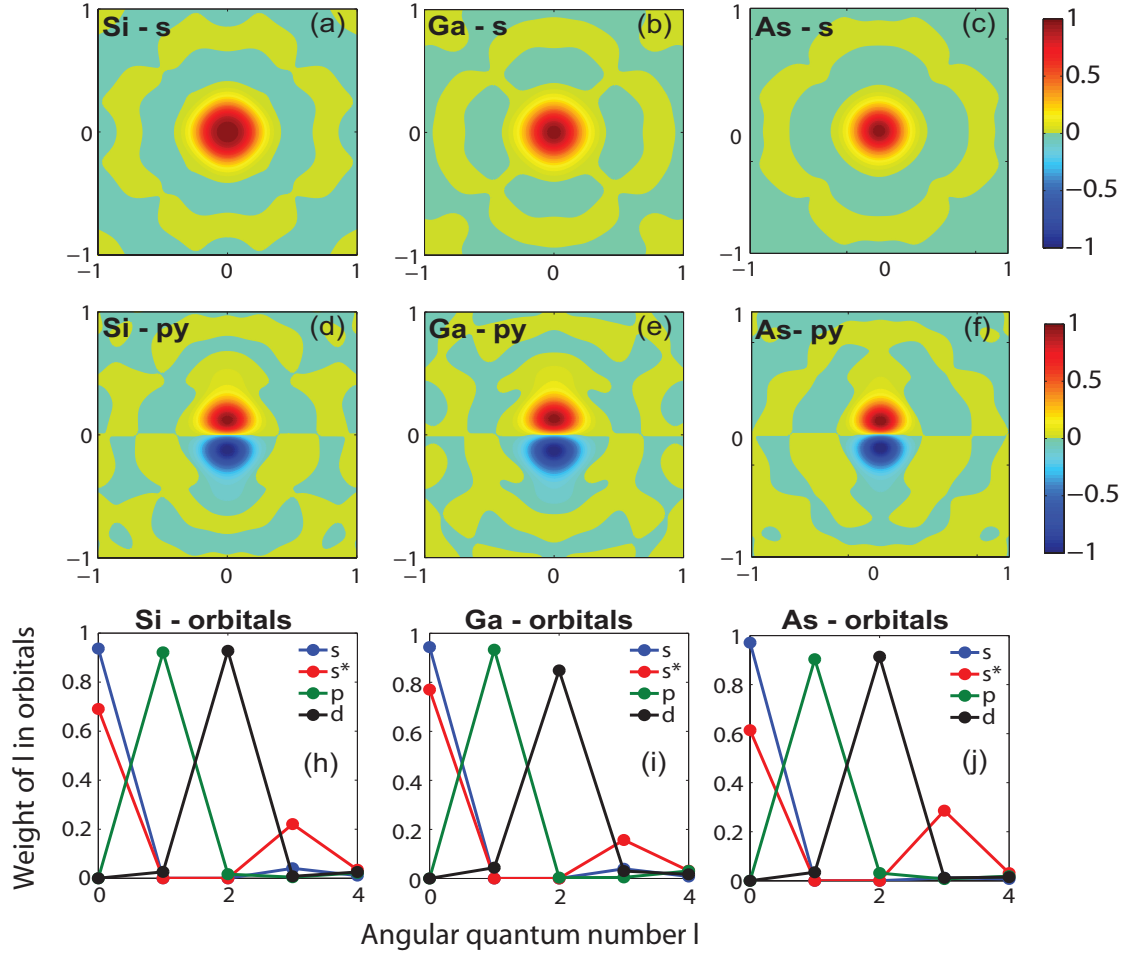


FIG. 5: Contours of selected ETB basis functions of Si ((a),(d)), Ga ((b),(e)) and As ((c),(f)) atoms. (a),(b) and (c) correspond to the contours of  $s$  orbitals of Si, Ga and As atoms in x-y plane. (d),(e) and (f) correspond to the contours of  $p_y$  orbitals of Si, Ga, and As atoms. (g),(h) and (i) show the contribution of different angular momentums in basis functions of Si, Ga, and As atoms. The ETB basis functions of Si and GaAs are highly localized basis functions with one dominant angular momentum.

diamond structures.

## B. Application to UTBs

To validate the transferability of the ETB model, band structures and eigen functions of [001] UTBs passivated by Hydrogen atoms are calculated by both HSE06 and ETB models. The current calculations assume no strain in the UTBs. In the HSE06 calculations, charged hydrogen atoms are used to passivate the dangling bonds of the surface atoms in GaAs UTBs. The surface As and Ga atoms are passivated by charged hydrogen atoms with  $3/4$  (denoted by  $H_c$ ) and  $5/4$  (denoted by  $H_a$ ) electron respectively. The charged hydrogen atoms neutralize most of the surface induced electric field in the UTBs. As a result, the charge distribution and local potential shows almost flat envelopes inside the UTBs. Small deviation of potential can only be observed at the surface Si/Ga/As atoms. The nearly flat potential envelope suggests geometry dependent build-in potentials are needed only for surface atoms. Thus the comparisons between

self-consistent hybrid functional calculations and single shot ETB calculations are fair.

The HSE06 calculations show that the Hydrogen orbitals contribute to the deep valence bands, thus Hydrogen atoms are considered explicitly into the ETB Hamiltonian of UTBs in this work.  $1s$  orbital is used as the ETB basis function for Hydrogen atoms. The explicit passivation model include extra Slater Koster type ETB parameters  $E_{s_H s}$ ,  $V_{s_H s \sigma}$ ,  $V_{s_H p \sigma}$ ,  $V_{s_H s^* \sigma}$  and  $V_{s_H d \sigma}$ . Furthermore, a geometry and element dependent potential  $\delta$  is included for surface atoms. The onsite energies of the surface atoms are shifted by  $\delta$ . The onsite energy of the surface Ga atoms are thus  $E_{\alpha_c} + \delta_{H_c}$ ; and for surface As atoms, the onsite energies are  $E_{\alpha_a} + \delta_{H_c}$ . Here the  $\alpha$  stands for  $s, p, d$  and  $s^*$  orbitals. ETB parameters of Si/GaAs in Si/GaAs UTBs are identical with the parameters of unstrained bulk materials provided in section III A.

To determine the ETB parameters of H-passivation, band structures and real space wave functions of selected

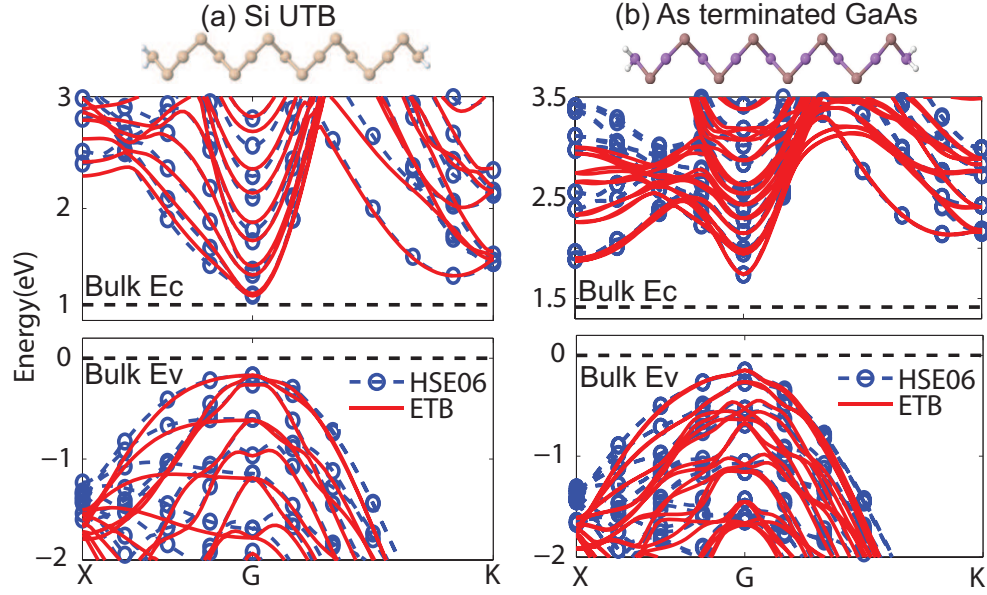


FIG. 6: Band structures of 001 Si (a) and As terminated GaAs (b) UTBs by ETB agree with HSE06 band structures, demonstrating the bulk Si and GaAs ETB parameters are transferable to UTB cases. All UTBs contain 17 non-Hydrogen atomic layers (with thickness  $4a_0$ ).

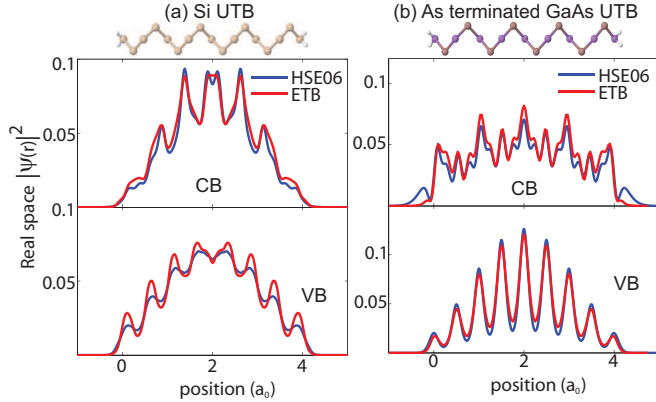


FIG. 7: Planar averaged real space probability amplitudes of lowest conduction and topmost valence states of 001 Si (a) and As terminated GaAs UTBs (b) by HSE06 and ETB calculations. With the real space TB basis functions, the real space probability amplitudes of TB calculations show reasonable agreement with the HSE06 probability amplitudes. UTBs contain 17 non-Hydrogen atomic layers (with thickness  $4a_0$ ).

bands near the Fermi level of the UTBs are considered as fitting targets. The inclusion of wave functions as targets serves the purpose of correcting possible problematic states. The target Si/GaAs UTBs contain 17 non-Hydrogen atomic layers. Parameters for Hydrogen atoms are also shown in table I. In GaAs UTBs, As and Ga are passivated by Hydrogen atoms with different charge, thus the Hydrogen atoms have different onsite energies when different types of atoms are passivated. The Hydro-

gen atoms bonding with As atoms are charged positively while the ones bonding with Ga atoms are charged negatively. Consequently, the  $H_c$  which forms bond with As have a higher onsite energy than the  $H_a$  which forms bond with Ga.

Band structures of Si/GaAs UTBs are shown in Fig. 6. The ETB band structures match the HSE06 band structures well for energies ranging from 1eV below the topmost valence bands to 1eV above the lowest conduction bands. Using the explicit ETB basis functions, ETB wave functions of UTBs with subatomic resolution are obtained and can be compared with corresponding HSE06 wave functions. Planar averaged probability amplitudes of wave functions of the lowest conduction band and top most valence bands in Si/GaAs UTBs are shown in Fig. 7. It can be seen that not only the envelope but also details in subatomic resolution of the ETB planar averaged  $|\psi|^2$  show agreement with corresponding HSE06 results. On the other hand, Fig. 8 compares the ETB atom site resolved probability amplitudes among ETB models in present and previous works (Ref.11,27). The cations and anions in GaAs UTBs form different envelopes for all of the presented states. The lowest conduction and highest valence states turn out to be well confined states in Si UTBs in all of the calculations. While, in GaAs UTBs, the lowest conduction states has significant contribution from the surface atoms. In Si ETB probability amplitudes by previous parametrizations show similar envelopes compared to the ETB and HSE06 probability amplitudes in this work. Fig. 8 (d) shows the problematic valence states in As terminated GaAs UTB by parameters of previous work. The corresponding valence states by this work turn out to be a well confined ones.



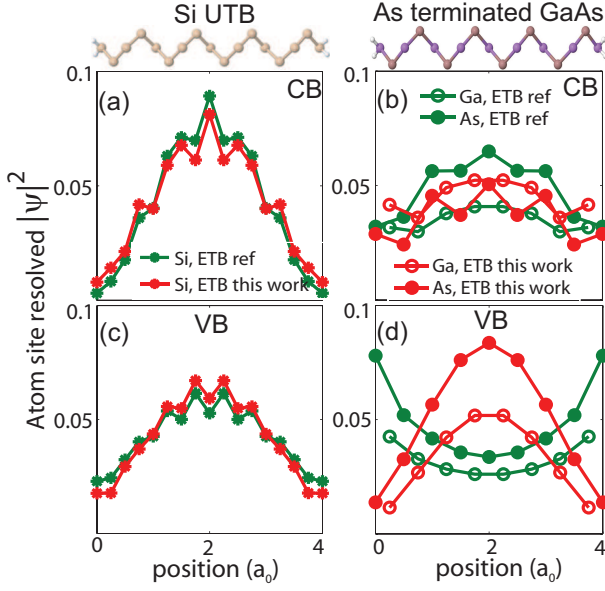


FIG. 8: ETB atom site resolved probability amplitudes of Si ((a),(c)), and As terminated GaAs ((b),(d)) UTBs using ETB parameters in this work and previous work.<sup>11,27</sup> The ETB atom site probability using different parameters are qualitatively similar in Si UTB, while the ETB atom site probability in As GaAs are more sensitive to the parameter sets and passivation models, i.e. the valence states with parameters and passivation model by previous work are not confined. UTBs contain 17 atomic layers (thickness is  $4a_0$ ).

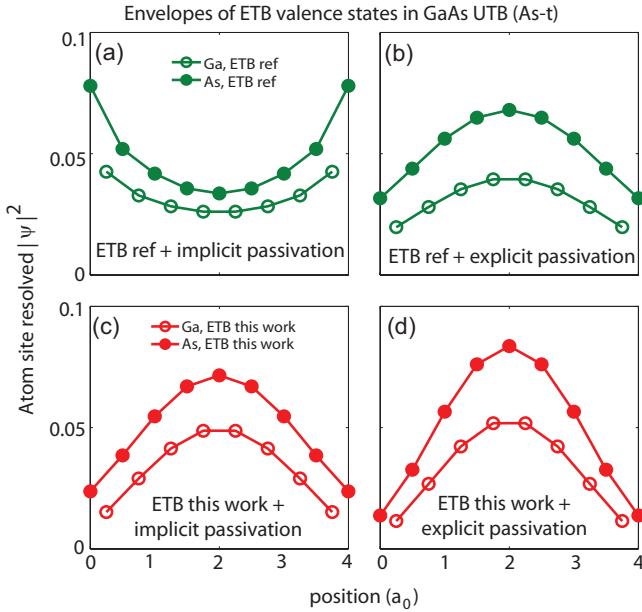


FIG. 9: Comparison of ETB wave functions using different ETB parameters and passivation model. (a) and (b) use ETB parameters in ref. 11. (c) and (d) use ETB parameters in this work. (a) and (c) correspond to implicit passivation model<sup>12</sup>; (b) and (d) correspond to explicit passivation model. The ETB parameters with the explicit passivation model shows the most confined states, while the previous parameters and implicit passivation model lead to less confined states.

To investigate this issue in more detail, in Fig. 9, ETB atom site resolved probability amplitudes for the top-most valence states of the four possible As-terminated GaAs UTBs are plotted: (a) previous parameters<sup>11</sup> and implicit passivation<sup>12</sup>; (b) previous parameters and explicit passivation; (c) new parameters and implicit passivation; (d) new parameters and explicit passivation. It is clear that, for a given set of bulk parameters, the implicit passivation model leads to wavefunctions that are less-confined than those of the explicit passivation model. On the other hand, with the same passivation model, the ETB parameters by this work shows more confined top valence states than the existing ETB parameters. Thus the un-confined ETB state using the existing parameter set and implicit passivation model appears to be due to both the bulk GaAs parameters and the passivation model. The implicit model<sup>12</sup> replaces the  $s$ - and  $p$ -orbitals of the surface atoms by  $sp^3$  hybrids and raises the energy of the dangling hybrids by  $\delta_{sp^3} = 30\text{eV}$ . The  $d$ - and  $s^*$ -orbitals are left completely un-passivated, and the unconfined states of Fig. 9 (a) are only slightly affected by changing the value of  $\delta_{sp^3}$ . The impact of alternate implicit passivation model to explicit passivation model is obvious by comparing sub-figures (a) to (b), as well as (c) to (d). To better understand the role of bulk parameters to this behavior, we experimented by reducing the magnitude of the nearest-neighbor  $p_a$ - $d_c$  coupling parameters in both sets as  $V_{p_a d_c \sigma} \rightarrow V_{p_a d_c \sigma} + 0.3\text{eV}$ ,  $V_{p_a d_c \pi} \rightarrow V_{p_a d_c \pi} - 0.3\text{eV}$ . Remarkably, in both cases the topmost valence-band state became much more confined. Bulk valence band wave functions in modified and original parameter sets tell the story: The general trend is that bulk sets which generate more  $p$ -like top of VB states give better confinement under passivation (and especially implicit passivation) than do those with higher  $d$ -content. The reduction of  $|V_{p_a d_c \sigma}|$  and  $|V_{p_a d_c \pi}|$  lead to more  $p$ -like top VB states. Ga terminated case has less passivation problems because its top-of-VB bulk states have more contribution from the As atoms than from the Ga atoms.

Fig. 10 shows the band gaps of the Si and GaAs [001] UTBs as functions of UTB thickness. With the ETB parameters by this work, the ETB bandgaps of Si and GaAs UTBs with thickness from 0.5nm to 4nm agree well with the gaps by HSE06 calculations. The ETB bandgaps of Si UTBs using parameters from previous work also show good agreement with the HSE06 results. However the ETB bandgaps of GaAs UTBs terminated with Ga and As atoms by previous parameterizations and implicit passivation model are of around 20% lower than the Hybrid functional results. The gaps of GaAs UTBs terminated with Ga and As atoms are very close in value for both Hybrid functional and ETB results in this work, however the gaps of GaAs UTBs terminated with Ga and As atoms by previous parameterizations and implicit passivation model show 0.1 to 0.2eV discrepancies. The band gap change in Si UTBs thicker than 3nm can be model by effective mass model (assuming parabolic E-k relation). While in the GaAs

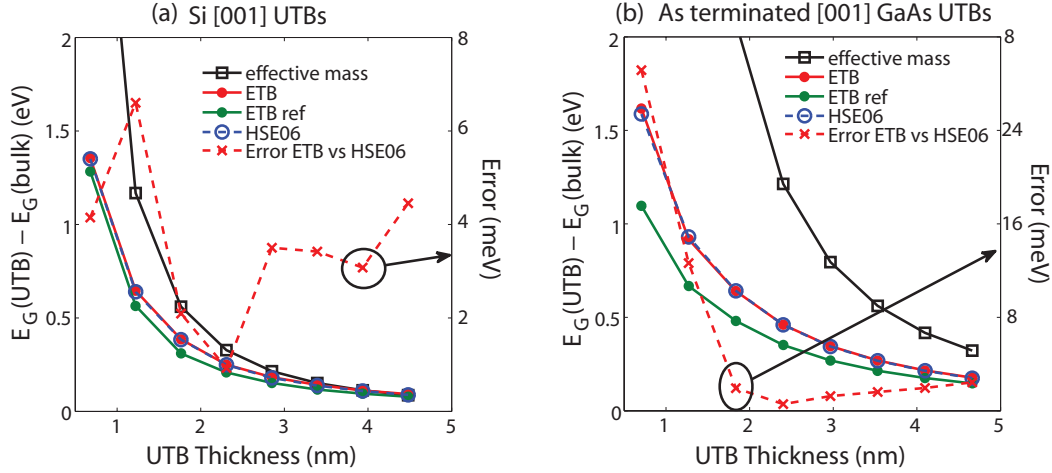


FIG. 10: Band gaps of Si UTBs (a) and As terminated UTBs (b) by HSE06 and ETB calculations. For the presented UTBs with thickness ranging from 1nm to 4.5nm, the ETB band gaps have discrepancies of less than 10meV compared with HSE06 ones. The band gap changes by effective mass calculation show agreement with HSE06 for Si UTBs thicker than 3nm. While the effective mass calculations has obvious discrepancies for all GaAs UTBs. The HSE06 and ETB calculations using parameters by this work consider Hydrogen atoms explicitly, while the ETB calculations using parameters by previous work is based on implicit passivation model.<sup>12</sup>

UTBs, the discrepancies between effective mass calculations and HSE06 or TB calculations are obvious for all GaAs UTBs presented, suggesting the non-parabolic feature of the GaAs valleys have significant impact to GaAs nano structures. The gaps by previous parameterization with implicit passivation model of As terminated GaAs UTBs has lower confined energies due to the unconfined valence states.

#### IV. CONCLUSION

It has been shown that the existing ETB parameterization together with the implicit passivation model gives unphysical states in As terminated GaAs UTB calculations. A more reliable technique of *ab-initio* mapping which generates ETB parameters and basis functions from *ab-initio* is developed. The *ab-initio* mapping process is applied to both bulk Si and GaAs. Slater Koster type ETB parameters within 1st nearest neighbour approximation and highly localized ETB basis functions are

obtained. The ETB parameters and basis functions of Si and GaAs are validated in corresponding UTB systems with passivation models that consider Hydrogen atom explicitly. Band gaps in Si and GaAs UTBs with different thickness are also calculated by HSE06, ETB and effective mass model. Compared with the existing ETB parameterizations and implicit passivation model, the ETB calculations in this work show good agreements with HSE06 calculations in both band structures and wave functions. This work shows that the ETB parameters by *ab-initio* mapping have good transferability. The mapping method developed here significantly reduces the uncertainty in both bulk and passivation models.

#### Acknowledgments

nanoHUB.org computational resources operated by the Network for Computational Nanotechnology funded by NSF are utilized in this work. Evan Wilson from Network for Computational Nanotechnology, Purdue University is acknowledged for improving the manuscript.

\* Electronic address: tyhua02@gmail.com

- <sup>1</sup> Y. K. Choi, K. Asano, N. Lindert, V. Subramanian, T. J. King, J. Bokor, and C. Hu, IEEE Electron Device Lett **21**, 254 (2000).
- <sup>2</sup> D. Hisamoto, C. Lee, W. J. Kedzierski, H. Takeuchi, K. Asano, C. Kuo, E. Anderson, J. King, T. J. Bokor, and C. Hu, IEEE Electron Device Lett **24**, 2320 (2000).
- <sup>3</sup> Y. Xuan, W. Lu, Y. Hu, H. Yan, and M. Lieber, C, Nature **441**, 489 (2006).
- <sup>4</sup> R. Hatcher and C. Bowen, Applied. Phys. Lett **103**, 162107 (2013).
- <sup>5</sup> A. Krukau, O. Vydrov, A. Izmaylov, and G. Scuseria, J.

- Chem. Phys. **124**, 224106 (2006).
- <sup>6</sup> M. S. Hybertsen and S. G. Louie, Phys. Rev. B **34**, 5390 (1986).
- <sup>7</sup> S. Ismail-Beigi and S. G. Louie, Phys. Rev. Lett. **90**, 076401 (2003).
- <sup>8</sup> G. Klimeck, F. Oyafuso, T. B. Boykin, C. R. Bowen, and P. V. Allmen, Computer Modeling in Engineering and Science (CMES) **3**, 601 (2002).
- <sup>9</sup> R. Lake, G. Klimeck, and S. Datta, Phys. Rev. B **47**, 6427 (1993).
- <sup>10</sup> J.-M. Jancu, R. Scholz, F. Beltram, and F. Bassani, Phys. Rev. B **57**, 6493 (1998).

- <sup>11</sup> T. B. Boykin, G. Klimeck, R. C. Bowen, and F. Oyafuso, Phys. Rev. B **66**, 125207 (2002).
- <sup>12</sup> S. Lee, F. Oyafuso, P. von Allmen, and G. Klimeck, Phys. Rev. B **69**, 045316 (2004).
- <sup>13</sup> N. Marzari and D. Vanderbilt, Phys. Rev. B **56**, 12847 (1997).
- <sup>14</sup> I. Souza, N. Marzari, and D. Vanderbilt, Phys. Rev. B **65**, 035109 (2001).
- <sup>15</sup> X. Qian, J. Li, L. Qi, C.-Z. Wang, T.-L. Chan, Y.-X. Yao, K.-M. Ho, and S. Yip, Phys. Rev. B **78**, 245112 (2008).
- <sup>16</sup> W. C. Lu, C. Z. Wang, T. L. Chan, K. Ruedenberg, and K. M. Ho, Phys. Rev. B **70**, 041101 (2004).
- <sup>17</sup> A. Urban, M. Reese, M. Mrovec, C. Elsässer, and B. Meyer, Phys. Rev. B **84**, 155119 (2011).
- <sup>18</sup> Y. Tan, M. Povolotskyi, T. Kubis, Y. He, Z. Jiang, G. Klimeck, and T. Boykin, Journal of Computational Electronics **12**, 56 (2013), ISSN 1569-8025.
- <sup>19</sup> Z. Jiang, M. A. Kuroda, Y. Tan, D. M. Newns, M. Povolotskyi, T. B. Boykin, T. Kubis, G. Klimeck, and G. J. Martyna, Applied Physics Letters **102**, 193501 (2013), ISSN 0003-6951.
- <sup>20</sup> J. C. Slater and G. F. Koster, Phys. Rev. **94**, 1498 (1954).
- <sup>21</sup> A. V. Podolskiy and P. Vogl, Phys. Rev. B **69**, 233101 (2004).
- <sup>22</sup> Y.-S. Kim, K. Hummer, and G. Kresse, Phys. Rev. B **80**, 035203 (2009).
- <sup>23</sup> N. Ashcroft and N. Mermin, *Solid State Physics* (Saunders College, Philadelphia, 1976).
- <sup>24</sup> P.-O. Lowdin, J. Chem. Phys. **18**, 56 (1950), ISSN 365.
- <sup>25</sup> L. Zeng, Y. He, M. Povolotskyi, X. Liu, G. Klimeck, and T. Kubis, Journal of Applied Physics **113**, 213707 (2013).
- <sup>26</sup> G. Kresse and J. Furthmüller, Computational Materials Science **6**, 15 (1996).
- <sup>27</sup> T. B. Boykin, G. Klimeck, and F. Oyafuso, Phys. Rev. B **69**, 115201 (2004).